Compensation of thermal nonlinearity effect in optical resonators

Ivan Grudinin,[1,2] Hansuek Lee,[1,2] Tong Chen,[1] and Kerry Vahala[1,*]

[1]*Department of Applied Physics, Caltech, 1200 E. California Blvd., Pasadena, 91125 CA, USA*
[2]*Equal contributions*
[*]vahala@caltech.edu

Abstract: Thermal nonlinearity is known to cause bistability in Whispering Gallery Mode (WGM) resonators and to destabilize the red slope of the Lorentzian resonant curve. We demonstrate an optical technique that allows compensation of the thermal effect and forces the resonances to appear linear with both red and blue slopes stable.

References and links

1. K. J. Vahala, "Optical microcavities," Nature **424**(6950), 839–846 (2003).
2. S. M. Spillane, T. J. Kippenberg, K. J. Vahala, K. W. Goh, E. Wilcut, and H. J. Kimble, "Ultrahigh-Q toroidal microresonators for cavity quantum electrodynamics," Phys. Rev. A **71**(1), 013817 (2005).
3. T. Aoki, B. Dayan, E. Wilcut, W. P. Bowen, A. S. Parkins, T. J. Kippenberg, K. J. Vahala, and H. J. Kimble, "Observation of strong coupling between one atom and a monolithic microresonator," Nature **443**(7112), 671–674 (2006).
4. T. J. Kippenberg and K. J. Vahala, "Cavity opto-mechanics," Opt. Express **15**(25), 17172–17205 (2007).
5. V. S. Ilchenko and A. B. Matsko, "Optical resonators with whispering-gallery modes-part II: Applications," IEEE J. Sel. Top. Quantum Electron. **12**(1), 15–32 (2006).
6. S. M. Spillane, T. J. Kippenberg, and K. J. Vahala, "Ultralow-threshold Raman laser using a spherical dielectric microcavity," Nature **415**(6872), 621–623 (2002).
7. T. J. Kippenberg, S. M. Spillane, and K. J. Vahala, "Kerr-nonlinearity optical parametric oscillation in an ultrahigh-Q toroid microcavity," Phys. Rev. Lett. **93**(8), 083904 (2004).
8. F. Vollmer and S. Arnold, "Whispering-gallery-mode biosensing: label-free detection down to single molecules," Nat. Methods **5**(7), 591–596 (2008).
9. V. S. Ilchenko and M. L. Gorodetskii, "Thermal nonlinear effects in optical whispering gallery microresonators," Laser Phys. **2**, 1004–1009 (1992).
10. T. Carmon, L. Yang, and K. J. Vahala, "Dynamical thermal behavior and thermal self-stability of microcavities," Opt. Express **12**(20), 4742–4750 (2004).
11. L. He, Y.-F. Xiao, C. Dong, J. Zhu, V. Gaddam, and L. Yang, "Compensation of thermal refraction effect in high-Q toroidal microresonator by polydimethylsiloxane coating," Appl. Phys. Lett. **93**(20), 201102 (2008).
12. H. S. Choi and A. M. Armani, "Thermal nonlinear effects in hybrid optical microresonators," Appl. Phys. Lett. **97**(22), 223306 (2010).
13. I. S. Grudinin and K. J. Vahala, "Thermal instability of a compound resonator," Opt. Express **17**(16), 14088–14097 (2009).
14. A. E. Fomin, M. L. Gorodetsky, I. S. Grudinin, and V. S. Ilchenko, "Nonstationary nonlinear effects in optical microspheres," J. Opt. Soc. Am. B **22**(2), 459–465 (2005).
15. A. C. Liu, M. J. F. Digonnet, and G. S. Kino, "Measurement of the dc Kerr and electrostrictive phase modulation in silica," J. Opt. Soc. Am. B **18**(2), 187–194 (2001).
16. M. Cai, O. Painter, and K. J. Vahala, "Observation of critical coupling in a fiber taper to a silica-microsphere whispering-gallery mode system," Phys. Rev. Lett. **85**(1), 74–77 (2000).
17. S. M. Spillane, T. J. Kippenberg, O. J. Painter, and K. J. Vahala, "Ideality in a fiber-taper-coupled microresonator system for application to cavity quantum electrodynamics," Phys. Rev. Lett. **91**(4), 043902 (2003).

1. Introduction

Whispering Gallery Mode (WGM) resonators have numerous applications in science and technology [1], including cavity QED [2,3], cavity optomechanics [4] nonlinear optics [5–7] and biosensing [8]. Thermal nonlinearity (caused by light absorption in the WGM) is present in virtually every WGMR and is known to cause bistability [9] at high circulating power levels. Importantly, at room temperature it renders the lower frequency slope (the "red" slope)

of the WGM resonance unstable in silica resonators [10]. Observation of the actual line shape function must therefore occur at reduced power levels. Attempts have been made to cancel or reduce the thermal effect [11,12] at the expense of the optical quality factor. In this contribution we demonstrate a technique that allows one to cancel thermal nonlinearity in a WGM of choice using another WG mode in the same resonator as a stabilizer. We demonstrate the method by cooling a mechanical mode of the resonator through red detuning of a pump wave.

2. Theoretical model

Thermal shift of the optical resonator eigenfrequency is caused by the absorption of coupled laser power and subsequent heating. In WGM resonators the frequency shift $\Delta\omega$ is caused primarily by temperature dependence of refractive index n and thermal expansion α_T:

$$\frac{\Delta\omega}{\omega} = -\left(\frac{1}{n}\frac{\partial n}{\partial T} + \alpha_T\right)\Delta T = -\beta\Delta T \tag{1}$$

However, if another WGM in the same resonator is excited at a different wavelength by a second laser and if this laser is thermally locked [10] on the stable "blue" slope, then the optical pumping of the original WGM can be stabilized. Before describing experimental results, we first detail the numerics used to study the stabilization mechanism. A simplified model is also described in section A. The system consists of a cavity with two WGM resonances at different wavelengths, but sharing approximately the same volume. A system of coupled equations similar to those in [13,14] is used to analyze the thermal behavior. Table 1 lists the variables and definitions. Subscripts "a" and "b" denote the parameters of the corresponding resonator modes.

Table 1. Parameters and variables used in computation of resonance curves in Fig. 2

Parameter, notation	Value
Optical quality factor, Q	$Q_a = 1.4 \times 10^7$, $Q_b = 7 \times 10^6$
Density, ρ	2.2 g/cm^3
Thermal conductivity, k	1.4×10^5 erg/(cm K s)
Heat capacity, C	6.7×10^6 erg/(g K)
Thermal diffusivity, D	$D = k/(\rho C) = 9.5 \times 10^{-3}$ cm^2/s
Third order susceptibility, $\chi^{(3)}$	1.3×10^{-14} cm^3/erg (esu) [15]
Absorption coefficient, α	5×10^{-4} cm^{-1}
Thermal expansion and thermorefractivity, β	8.83×10^{-6} K^{-1}
Refractive index, n	1.444
Laser wavelength, λ	1540, 1450 nm
Resonator major radius, R	29 μm
Speed of light in vacuum, c	29979245800 cm/s
WGM eigenfrequencies, $\omega_{a,b}$,	Variables
WGM volumes, $V_{a,b}$. (l,m are WGM indices)	$V = 3.9R^{(11/6)}(2\pi c/(\omega n))^{(7/6)}\sqrt{l-m+1}$
WGM optical loss rates, $\gamma_{a,b}$	$\gamma = \omega/(2Q)$
Pump power from laser 1 and 2, $W_{1,2}$	erg/s
Generalized force created by lasers 1 and 2	$F_{1,2} = \sqrt{2\pi\omega_{1,2}W/(n^2 V_{a,b}Q_{a,b})}$
Kerr and thermal nonlinearity, μ and ν	$\mu = 2\pi\chi^{(3)}/n^2$ and $\nu = n\alpha c/(4\pi C\rho)$
Thermal relaxation rate of the resonator	$\delta_\theta = D/(R/4)^2$

We describe the electric field of the WGMs using the rotating wave approximation:

$$\vec{E}(\vec{r},t) = a(t)\vec{E}_0(\vec{r})e^{i\omega t}, \tag{2}$$

where the field distribution of a mode is normalized so that

$$\int \left|\overrightarrow{E_0}\right|^2 d\vec{r} = 1. \qquad (3)$$

We introduce the equations describing the dynamics of the slowly varying amplitudes **a** and **b** in cgs units as

$$\begin{cases} \dot{a} + a(\gamma_a + i[\omega_1 - \omega_a(1 - \mu|a|^2 - \beta\theta)]) = iF_1 \\ \dot{b} + b(\gamma_b + i[\omega_2 - \omega_b(1 - \mu|b|^2 - \beta\theta)]) = iF_2. \\ \dot{\theta} + \delta_\theta\theta = \nu(|a|^2 + |b|^2) \end{cases} \qquad (4)$$

Here $\theta = \int (T - T_0)\left|\overrightarrow{E_0(\vec{r})}\right|^2 \overrightarrow{dr}$ is the relative temperature averaged over the volume of the modes (assumed equal for the two WGMs). The WGM volume formula given in Table 1 is an approximation computed for a sphere, and numerical simulations or other approximations may be used for spheroidal resonators. The thermal nonlinearity observed in the experiment is a result of mutual dynamics of the laser's frequency scan and laser induced eigenfrequency $\theta = y_5\theta_c$, change in the WGM. The effective time constant of the thermal nonlinearity depends on the laser scan rate. Static behavior of the resonator corresponds to the longest time constant describing thermal relaxation of the whole resonator.

2.1 Solution of the nonlinear system

To deal with the complex numbers in Eqs. (4), field amplitudes are defined as $a = a_1 + ia_2$ and $b = b_1 + ib_2$. We look for the solutions in which a_1, a_2, b_1, b_2 are real:

$$\begin{cases} \dot{a}_1 = -a_1\gamma_a + a_2(\omega_1 - \omega_a(1 - \mu|a|^2 - \beta\theta)) \\ \dot{a}_2 = -a_2\gamma_a - a_1(\omega_1 - \omega_a(1 - \mu|a|^2 - \beta\theta)) + F_1 \\ \dot{b}_1 = -b_1\gamma_b + b_2(\omega_2 - \omega_b(1 - \mu|b|^2 - \beta\theta)) \\ \dot{b}_2 = -b_2\gamma_b - b_1(\omega_2 - \omega_b(1 - \mu|b|^2 - \beta\theta)) + F_2 \\ \dot{\theta} = \nu(a^2 + b^2) - \delta_\theta\theta \end{cases} \qquad (5)$$

In order to accommodate both very large and very small quantities in a numerical solver we use non-dimensional variables. The following substitutions are made in Eqs. (5): $a_1 = y_1 a_c$, $a_2 = y_2 a_c$, $b_1 = y_3 b_c$, $b_2 = y_4 b_c$, $t = \tau t_c$, and $\Delta\omega_{a,b} = \omega_{1,2} - \omega_{a,b}$ where $a_c = \sqrt{\dfrac{\gamma_a}{\omega_a\mu}}, b_c = \sqrt{\dfrac{\gamma_a}{\omega_b\mu}}$, $\theta_c = \dfrac{\gamma_a}{\omega_a\beta}$, and $t_c = \dfrac{1}{\gamma_a}$. With these substitutions, the equations contain only dimensionless values which are close to unity in magnitude (derivatives here are with respect to τ):

$$\begin{cases} \dot{y}_1 = -y_1 + y_2\Delta\omega_a/\gamma_a + y_2y_1^2 + y_2^3 + y_2y_5 \\ \dot{y}_2 = -y_2 - y_1\Delta\omega_a/\gamma_a - y_1^3 - y_1y_2^2 - y_1y_5 + F_1\sqrt{\mu\omega_a/\gamma_a^3} \\ \dot{y}_3 = -y_3\gamma_b/\gamma_a + y_4\Delta\omega_b/\gamma_a + y_4y_5\omega_b/\omega_a + y_4y_3^2 + y_4^3 \\ \dot{y}_4 = -y_4\gamma_b/\gamma_a - y_3\Delta\omega_b/\gamma_a - y_3y_5\omega_b/\omega_a - y_3^3 - y_3y_4^2 + F_2\sqrt{\mu\omega_b/\gamma_a^3} \\ \dot{y}_5 = -y_5\delta_\theta/\gamma_a + (y_1^2 + y_2^2)\nu\beta/(\mu\gamma_a) + (y_3^2 + y_4^2)\nu\beta\omega_a/(\mu\gamma_a\omega_b) \end{cases} \qquad (4')$$

We set all time derivatives to zero and find the static solutions of the system (4′) using the numerical solver Maple. The power circulating in resonator mode "a", for example, can be estimated as

$$P_{circ} = (y_1^2 + y_2^2)a_c^2 \frac{ncV_a}{(2\pi)^2 R} \times 10^{-7} [Watt]. \tag{6}$$

We also check the static solutions for stability against minor deviations of variables y_i in the Lyapunov sense. Stability analysis is performed as previously described in [13]. To model the experimental outcomes, we fix the frequency of the first laser ω_1 and scan the frequency of the second laser to observe the stabilization effect, as shown in the next section. We disregard the cross-mode modulation via the Kerr effect as the thermal effect is the dominant nonlinearity in our case.

3. Experimental verification

We use two New Focus velocity lasers to probe the resonator. The stabilizing laser (ω_1, $\lambda_1 \approx 1550nm$) excites the WGM at $\lambda = 1543.2$ nm and the probing laser (ω_2, $\lambda_1 \approx 1450nm$) operates at $\lambda = 1433.3$ nm. We use a WDM coupler to combine the two lasers and to separate the optical signals passing through the resonator. A tapered fiber coupler [16,17] is used to excite the WGMs of an ellipsoidal resonator with a major radius of 29 micrometers fabricated on a silicon chip. Experimental setup diagram is shown on Fig. 1.
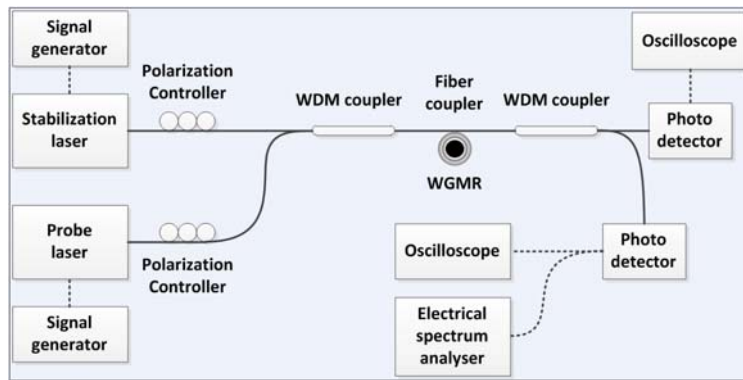

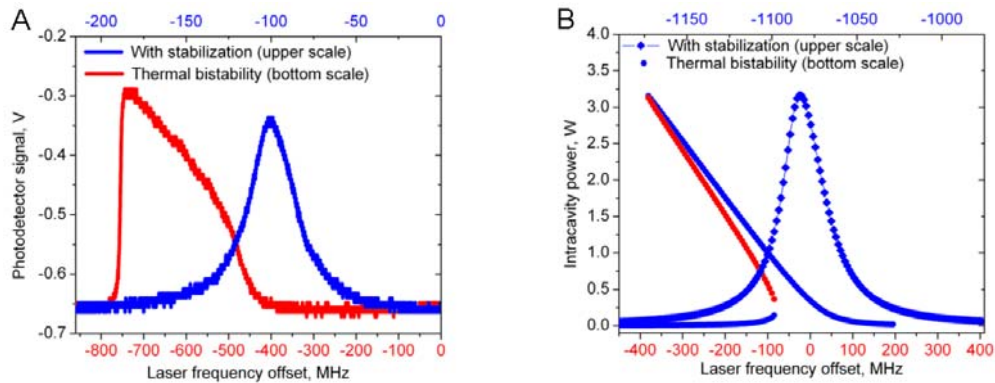Fig. 1. Schematic of the experimental setup.

Fig. 2. A) experimental frequency scans of a WGM resonance at 1450 nm without (red) and with stabilization (blue). B) solutions of the system (4). WGM resonance with thermal effect (red dots show unstable solutions). Solutions for the same mode when the stabilizing laser is activated constitute a nearly Lorentzian lineshape. Note the frequency shift of the stabilized resonance caused by heating from the stabilizing WGM.

During the experiment we first scan the 1450 nm laser alone over the resonance and record the resonance with the thermal nonlinearity (red trace on the left panel of Fig. 2). The shape of this resonance is slightly different from the static solution due to dynamic effects. We then

activate the stabilizing laser at 1550 nm and thermally lock it to the blue slope of the nearby resonance. Heating from this laser causes the 1450 nm resonance to shift by a value that depends on the pump power. With the stabilizing laser enabled, the 1450 nm WGM exhibits a more Lorentzian lineshape (blue trace on the left panel of Fig. 2).

The vertical axis of the right panel gives the calculated circulating power for the experimental conditions: coupled power of 300 µW at 1550 nm, and 130 µW at 1450 nm; and loaded quality factors of 1.4×10^7 and 7×10^6, respectively.

If the Q of both modes is similar, a much higher coupled power (relative to the probe power of the stabilized mode) is required. In well fabricated WGMs, especially in spheroidal ones, most modes have high optical Q and it may be difficult to find a pair of modes with different Q. Nonetheless, the difference in Q can still be achieved by using an asymmetric coupling technique, wherein distinct transverse WGMs (different number of field maxima in vertical direction) are used. Such modes have maxima shifted in the vertical direction, enabling a strong difference in loaded Q of the two modes by a single taper waveguide. The modes in our experiment were, in fact, of a different order and the higher Q mode (3 maxima in vertical direction, l-m = 2) was more weakly loaded than the stabilized mode (2 maxima, l-m = 1). As shown in Fig. 2, the numerical model verifies the experimental results with good accuracy. The thermal relaxation rate was chosen to correspond to a quarter of resonator radius R to match experimental results.

We further tested the stability of the 1450nm mode by manually tuning the probing laser to the blue and red slopes. The induced stability allowed us to apply optomechanical cooling and amplification to a mechanical mode present in our optical resonator (symmetrically on both slopes of the optical resonance). Doing so in the unresolved sideband regime we obtained
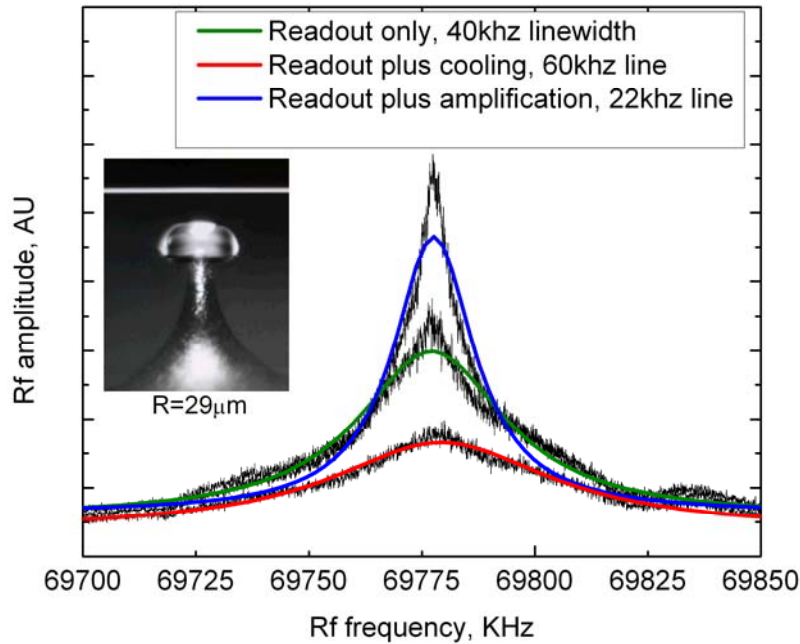

Fig. 3. Optical cooling and amplification of a 70 MHz mechanical mode of the optical resonator. Broadening and narrowing of the mechanical spectrum occurs due to optomechanical cooling and amplification in the unresolved sideband regime. Colored lines represent Lorentzian fits of the experimentally recorded spectra. Inset shows an optical photograph of the resonator near the fiber coupler.

modest but measurable cooling and amplification, as shown in Fig. 3. It is important to note that cooling (i.e., stable operation on the red slope) was not possible in the thermally unstabilized system.

To further explain the data presented in Fig. 3, laser light passing through the optical resonator is modulated by cavity vibrations which impose optical sidebands. These are demodulated by a photodetector, which provides an electronic signal with signatures of the mechanical resonances. This signal is then displayed by the electrical spectrum analyzer and the linewidth of the mechanical oscillator can be analyzed [4]. The spectra presented here were obtained by detecting the optical signal at 1550 nm that was thermally locked to the cavity resonance.

4. Conclusion

We have demonstrated an all-optical technique that makes it possible to counteract thermal nonlinearity in WGM resonators and makes the red slope of the resonant curve accessible. To demonstrate the technique we have applied it to optical cooling of the mechanical mode of an optomechanical resonator by pumping the resonator mode in the red detuned regime. This application to optomechanical cooling should be considered only illustrative as there are potential problems in applying the method to achieve large amounts of cooling. Among these is the onset of parasitic oscillation of mechanical modes as well as heating of the resonator by the stabilizing pump wave. Nonetheless, the method might find use in applications wherein it is necessary to observe stable resonances at higher power levels.

Appendix A. Analytical model

To understand the underlying stabilization mechanism, we develop a simple nonlinear dynamics model. In the case of a single WGM excitation, cavity heating by the pump laser depends on the pump power, the optical coupling efficiency, and detuning from the resonance frequency. Based on the conservation of energy, the net heating of the cavity is the laser pump heating (q_{in}) minus the thermal dissipation (q_{out}) [10]:

$$C\dot{\theta} = \dot{q}_{in} - \dot{q}_{out} = W_h \frac{1}{\left[(\omega_2 - \omega_{b,0}(1-\beta\theta))/\gamma_b\right]^2 + 1} - K\theta \text{. (A1)}$$

Here ω_2 is the laser frequency; $\omega_b = \omega_{b,0}(1-\beta\theta)$ is the resonance frequency; and we have defined the effective laser power $W_h = W\eta \frac{Q_{tot}}{Q_{abs}}$, where Q_{abs} is the absorption quality factor of the cavity and η is the coupling efficiency. The stability of WGM can be inferred by investigating the stability of the steady solution to Eq. (A1). The rearrangement of Eq. (A1) yields

$$\frac{C}{K}\left\{\left[\omega_2 - \omega_{b,0}(1-\beta\theta)\right]^2 + \gamma_b^2\right\}\dot{\theta} = f(\theta, \omega_2, W_h)$$

$$= -\beta^2\omega_{b,0}^2\theta^3 + 2\beta\omega_{b,0}(\omega_{b,0} - \omega_2)\theta^2 - \left[(\omega_2 - \omega_{b,0})^2 + \gamma_b^2\right]\theta + \gamma_b^2\frac{W_h}{K}$$

(A2)

The steady state solutions for $\dot{\theta} = 0$ and their stability can be determined from the phase diagram (Fig. 4). For blue detuning of the pump laser ($\omega_2 > \omega_b$), the monotonic form of $f(\theta, \omega_2, W_h)$ leads to a single, stable, steady state; whereas on red side ($\omega_2 < \omega_b$), thermal bistability may arise at sufficient pump power (W_h). The bistability would emerge as the saddle-node bifurcation when $\frac{W_h}{K}$ is above a certain threshold (i.e. large pump power or small
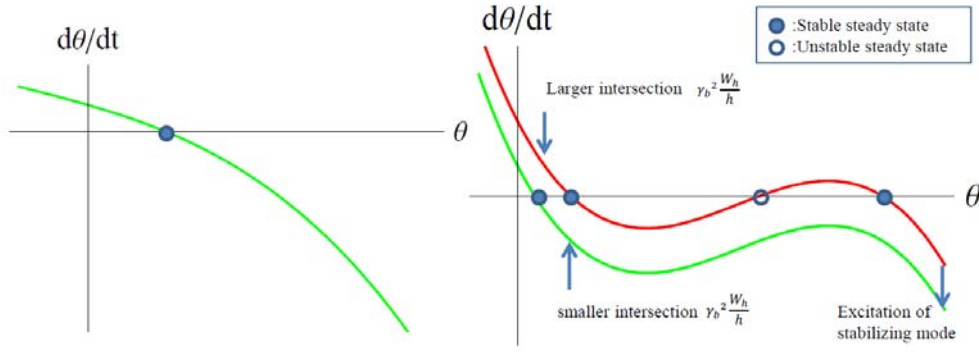
Fig. 4. Left panel: Phase diagram of temperature change of the cavity upon application of a blue detuned pump. There is always a single, stable steady-state solution. Right panel: Phase diagram of temperature change of the cavity upon using a red detuned pump. The thermal bistability may arise at sufficient pump power. The excitation of a stabilizing mode can compensate the nonlinearity via a saddle-node bifurcation.

thermal dissipation). In other words, the *increase* of thermal conductivity or the *decrease* of pump power would eliminate this bistability. In the present system, the blue-detuned excitation of another (stabilizing) WGM compensates the thermal nonlinearity by creating an "effective" enhancement to thermal conductivity. The stabilizing mode adds a second term to the dynamical equation as follows:

$$C\dot{\theta} = W_h \frac{1}{\left[(\omega_2 - \omega_b)/\gamma_b\right]^2 + 1} - K\theta + W_{s,c}(\theta) = W_{h,c}(\theta) - K\theta + W_{s,c}(\theta). \quad \text{(A3)}$$

Here, the effective laser power for the stabilizing mode, W_s is defined in the same fashion as W_h. $W_{s,c} = W_s / \left\{\left[(\omega_1 - \omega_a)/\gamma_a\right]^2 + 1\right\}$ and $W_{h,c} = W_h / \{[(\omega_2 - \omega_b)/\gamma_b]^2 + 1\}$ are the coupled power from the stabilizing and original pump mode. We are interested in the stabilizing effect of this additional term $W_{s,c}$ and explore stability of the steady state solutions θ_s of (A3) against small deviations. With a substitution of $\theta = \theta_s + \delta T$ into Eq. (A3) we get

$$C\delta\dot{T} = \frac{\partial W_{h,c}}{\partial \theta}\delta T - K\delta T + \frac{\partial W_{s,c}}{\partial \theta}\delta T = \frac{\partial W_{h,c}}{\partial \theta}\delta T - \left(K + \omega_a \beta \frac{\partial W_{s,c}}{\partial \omega_a}\right)\delta T \quad \text{(A4)}$$

When the stabilizing mode is excited on the blue side, the positive $\frac{\partial W_{s,c}}{\partial \omega_a}$ will effectively increase the thermal conductivity and eliminate the bistability via a saddle-node bifurcation. For the pump mode, $\frac{\partial W_{h,c}}{\partial \theta} = -\omega_b \beta \frac{\partial W_{h,c}}{\partial \omega_b}$ is negative on the blue slope and the solution is always stable. On the red slope, $\frac{\partial W_{h,c}}{\partial \theta}$ is positive and the coefficient of δT on the right hand side of (A4) must be negative to ensure the stability, leading to stability condition:

$$\left|\frac{\partial W_{h,c}}{\partial \theta}\right| < \left(K + \omega_a \beta \frac{\partial W_{s,c}}{\partial \omega_a}\right) \Rightarrow \omega_b \beta \left|\frac{\partial W_{h,c}}{\partial \omega_b}\right| < \left(K + \omega_a \beta \left|\frac{\partial W_{s,c}}{\partial \omega_a}\right|\right) \quad \text{(A5)}$$

For optimal pump detuning of the stabilizing mode (maximum value of $\left|\dfrac{\partial W_{s,c}}{\partial \omega_a}\right|$), we find

$\left|\dfrac{\partial W_{s,c}}{\partial \omega_a}\right|_{opt} = \dfrac{3\sqrt{3}}{4}\dfrac{W_s Q_a}{\omega_a}$, and the right hand side of Eq. (A5) has to be greater than the

maximum value of $\omega_a \beta \left|\dfrac{\partial W_{h,c}}{\partial \omega_b}\right|$. We finally get the stability condition:

$$\frac{3\sqrt{3}}{4}W_h Q_b < \frac{3\sqrt{3}}{4}W_s Q_a + \frac{K}{\beta}$$

Acknowledgments